



# SICPK27 cross-links SIHY5 and SIPIF4 in brassinosteroid-dependent photo- and thermo-morphogenesis in tomato

Changan Zhu<sup>a,1</sup>, Zhangjian Hu<sup>a,b,1</sup> , Chaoyi Hu<sup>a,b</sup>, Hongxue Ma<sup>a</sup>, Jie Zhou<sup>a,c</sup> , Xiaojian Xia<sup>a,c</sup> , Kai Shi<sup>a,c</sup> , Christine H. Foyer<sup>d</sup> , Jingquan Yu<sup>a,c,2</sup> , and Yanhong Zhou<sup>a,c,2</sup>

Affiliations are included on p. 11.

Edited by Chentao Lin, Fujian Agriculture and Forestry University, Fuzhou, China; received February 15, 2024; accepted July 16, 2024 by Editorial Board Member Joseph J. Kieber

**ELONGATED HYPOCOTOYL5 (HY5) and PHYTOCHROME INTERACTING FACTORS (PIFs) are two types of important light-related regulators of plant growth, however, their interplay remains elusive. Here, we report that the activated tomato (*Solanum lycopersicum*) HY5 (SIHY5) triggers the transcription of a Calcium-dependent Protein Kinase SICPK27. SICPK27 interacts with and phosphorylates SIPIF4 at Ser-252 and Ser-308 phosphosites to promote its degradation. SIPIF4 promotes hypocotyl elongation mainly by activating the transcription of *SIDWF*, a key gene in brassinosteroid (BR) biosynthesis. Such a SIHY5-SICPK27-SIPIF4-BR cascade not only plays a crucial role in photomorphogenesis but also regulates thermomorphogenesis. Our results uncover a previously unidentified mechanism that integrates Ca<sup>2+</sup> signaling with the light signaling pathways to regulate plant growth by modulating BR biosynthesis in response to changes in ambient light and temperature.**

photomorphogenesis | calcium-dependent protein kinase | light signal | brassinosteroid

Light is one of the most critical environmental cues that not only provides energy for photosynthesis but also regulates a variety of growth processes throughout the life cycle of plants (1). Upon seed germination in the soil, seedlings enact two intricate developmental programs, skotomorphogenesis, and photomorphogenesis, to thrive amid conditions of darkness and assorted luminosities, respectively (2). When seedlings emerge from the soil, light is perceived by plant photoreceptors, which inactivate CONSTITUTIVELY PHOTOMORPHOGENIC1 (COP1), a central repressor of photomorphogenesis (3). Functioning as an E3 ubiquitin ligase, COP1 targets many positive regulators of light signaling for degradation in darkness, including ELONGATED HYPOCOTOYL5 (HY5), which promotes photomorphogenesis in the light by regulating a wide range of genes directly or indirectly (4). On the other hand, light exposure results in the photoreceptor-dependent degradation of PHYTOCHROME INTERACTING FACTOR (PIF) proteins (5). It is well characterized that the phosphorylation status of PIF proteins determines their stability (6), therefore, unraveling kinases that phosphorylate PIFs in the light is important for optimizing the light signaling molecular framework. Calcium-dependent Protein Kinases (CPKs) are serine/threonine protein kinases, possessing a calcium-sensing protein domain and a kinase domain to directly translate Ca<sup>2+</sup> signals into downstream phosphorylation events (7). Given that light-induced changes in Ca<sup>2+</sup> influx from extracellular spaces into cytosol promote photomorphogenesis (8–10), CPKs might hold a pivotal position in the intricate interplay of light-Ca<sup>2+</sup> signal cross talk.

## SIHY5-Promoted SICPK27 Positively Regulates Photomorphogenesis

To determine whether tomato (*Solanum lycopersicum*) CPKs (SICPKs) are involved in light-induced Ca<sup>2+</sup> signal, we first examined how the transcript levels of 29 SICPKs are altered by light. RT-qPCR analysis showed that the transcription of *SICPK27* in 4-d-old seedlings was most significantly induced by white light (W) among the 29 SICPKs (SI Appendix, Fig. S1A). Moreover, exposure of germinated seeds to W, blue (B), red (R), and far-red (FR) light for 4 d all significantly increased transcript levels of *SICPK27* (Fig. 1A), along with reduced hypocotyl lengths compared with those in the dark (D) (SI Appendix, Fig. S1 B and C). In agreement with this, mutants of the FR light photoreceptor (*sphYA*), R light photoreceptor (*sphYB1B2*), R light and FR light photoreceptor (*sphYAB1B2*), and B light photoreceptor (*slcry1a*) all showed increased hypocotyl lengths (SI Appendix, Fig. S1 D and E) and decreased transcript levels of *SICPK27* relative to the wild type (WT) under W light (Fig. 1B).

## Significance

Phosphorylation is essential for the regulation of the development of plant seedlings, while the kinases responsible for photomorphogenic hypocotyl elongation are largely unknown. Here, we reveal that SIHY5 promotes the transcript accumulation of *SICPK27*, a Calcium-dependent Protein Kinase, which promotes seedling photomorphogenesis in the light. The *SICPK27* physically interacts with and phosphorylates SIPIF4 to promote its light-induced degradation, thereby repressing BR biosynthesis via modifying *SIDWF* transcript levels. This SIHY5-SICPK27-SIPIF4-BR light signal module also regulates thermal sensory hypocotyl growth, which grants plants the capacity and flexibility to optimize their growth and development in ever-changing environmental conditions.

Author contributions: J.Z., X.X., K.S., C.H.F., J.Y., and Y.Z. designed research; C.Z., Z.H., C.H., and H.M. performed research; Z.H. contributed new reagents/analytic tools; C.Z. analyzed data; and C.Z., J.Y., and Y.Z. wrote the paper.

The authors declare no competing interest.

This article is a PNAS Direct Submission. C.L. is a Guest Editor invited by the Editorial Board.

Copyright © 2024 the Author(s). Published by PNAS. This article is distributed under Creative Commons Attribution-NonCommercial-NoDerivatives License 4.0 (CC BY-NC-ND).

<sup>1</sup>C.Z. and Z.H. contributed equally to this work.

<sup>2</sup>To whom correspondence may be addressed. Email: jquy@zju.edu.cn or yanhongzhou@zju.edu.cn.

This article contains supporting information online at <https://www.pnas.org/lookup/suppl/doi:10.1073/pnas.2403040121/-/DCSupplemental>.

Published August 27, 2024.

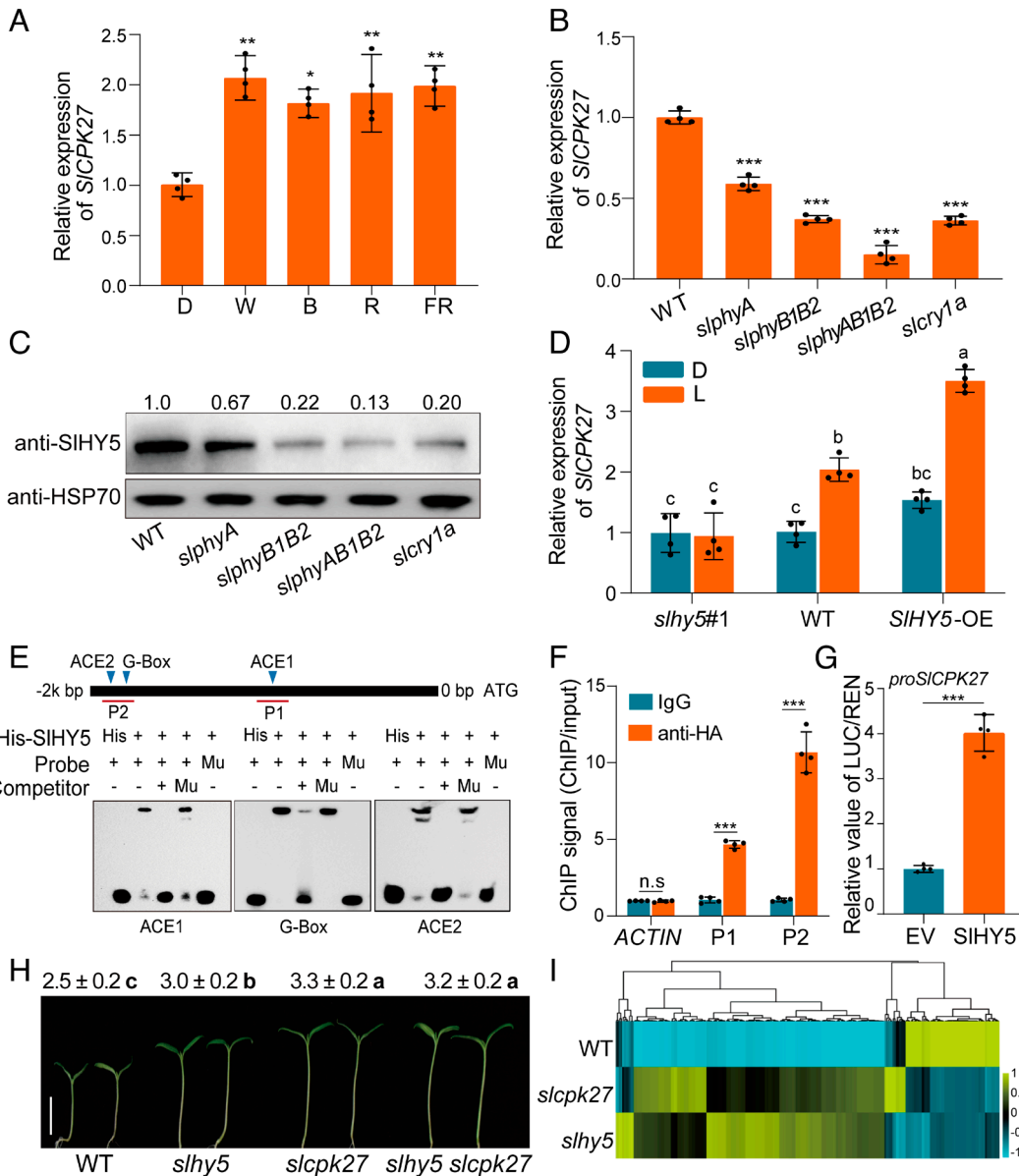


**Fig. 1.** SIHY5-regulated *SICPK27* plays a crucial role in photomorphogenesis. (A) Relative expression of *SICPK27* in 4-d-old wild-type (WT, Condone Red) seedlings grown in continuous dark (D), white light (W), blue light (B), red light (R), and far-red light (FR). Relative expression was calculated against the expression level in the dark, which was designated as 1. (B) Relative expression of *SICPK27* in 4-d-old WT (Moneymaker), FR light photoreceptor (*slphyA*), R light photoreceptor (*slphyB1B2*), R light and FR light photoreceptor (*slphyAB1B2*), and B light photoreceptor (*slcry1a*) mutant seedlings grown in continuous white light. Relative expression was calculated against the expression level in the WT, which was designated as 1. (C) Immunoblots showing SIHY5 protein levels of seedlings in (B). The relative levels of SIHY5, normalized to HSP70, were shown above the SIHY5 immunoblots. (D) Relative expression of *SICPK27* in 4-d-old *slhy5#1* mutant, WT (Ailsa Craig), and *SIHY5*-OE seedlings grown under continuous dark (D) and white light (L) conditions. Relative expression was calculated against the expression level of WT in the dark, which was designated as 1. (E) Diagram of *SICPK27* promoter region and EMSAs showing the binding ability of SIHY5 to *SICPK27* promoter. The blue deltas represented potential SIHY5 binding sites (ACE1, G-Box, ACE2). P1 and P2 indicate the promoter fragments identified by ChIP-qPCR. Competitors and mutant competitors were used at 100-fold. Mu, mutated probe in which the ACGT motif was changed to AAAA. (F) ChIP-qPCR analysis of SIHY5-binding ability to the promoter of *SICPK27* using 4-d-old *SIHY5*-OE seedlings grown in continuous light. (G) Dual-luciferase assays for the regulatory effect of SIHY5 on the expression of *SICPK27*. The ratio of LUC/REN of the EV (empty vector) was set as 1. (H) Hypocotyl phenotypes of 4-d-old WT (Condone Red), *slhy5*, *slcpg27*, and *slhy5 slcpg27* seedlings grown in continuous white light. The hypocotyl lengths above the graph are shown as mean  $\pm$  SD ( $n \geq 15$ ). (I) Heatmap analysis of *SICPK27*- and SIHY5-regulated genes. The bar represents the column z-score. Data are shown as mean  $\pm$  SD,  $n = 4$  in (A), (B), (D), (F), and (G). Different letters present differences according to ANOVA followed by Tukey's test ( $P < 0.05$ ) and asterisks represent significant differences compared with the WT or indicated control according to Student's t test (\* $P < 0.05$ , \*\* $P < 0.01$ , \*\*\* $P < 0.001$ ).

HY5 is a key transcription factor in light signaling, acting downstream of various photoreceptors and controlling the transcript of a number of light-responsive genes (11). While SIHY5 protein accumulated after exposure to W, B, R, and FR light (SI Appendix, Fig. S2A), this increase was greatly attenuated in photoreceptor mutants *slphyA*, *slphyB1B2*, *slphyAB1B2*, and *slcry1a* (Fig. 1C). We then compared the hypocotyl length and the transcript accumulation of *SICPK27* in the seedlings of *slhy5#1* mutants and *SIHY5*-over expression (*SIHY5*-OE) lines (Ailsa Craig

background) grown under W light. As shown in SI Appendix, Fig. S2 B and C, *slhy5#1* mutants showed longer while *SIHY5*-OE seedlings showed shorter hypocotyls relative to WT under W light. Notably, light-induced expression of *SICPK27* was compromised in the *slhy5#1* mutant but significantly increased in *SIHY5*-OE seedlings as compared with WT (Fig. 1D). To test whether SIHY5 directly regulates the expression of *SICPK27*, we performed electrophoretic mobility shift assays (EMSA) and found that His-tagged SIHY5 protein can bind to the promoter of *SICPK27*

at three different sites (Fig. 1E). Chromatin immunoprecipitation (ChIP) assays using light-grown *SIHY5*-OE seedlings confirmed the direct binding of SIHY5 to the both P1 and P2 regions of *SICPK27* promoter, with higher affinity to P2 in vivo (Fig. 1F). We further performed transient expression assays using a dual-luciferase (LUC) reporter system in *Nicotiana benthamiana* leaves, and the results showed that SIHY5 significantly enhanced the promoter activity of *SICPK27* (Fig. 1G). This implies that SIHY5 functions as the transcriptional activator of *SICPK27*.

To investigate whether *SICPK27* plays a role in photomorphogenesis, two homozygous lines, *slcpk27#2* and *slcpk27#6* (12), were grown in the dark or light conditions. The hypocotyl length of *slcpk27* mutants was similar to WT in the dark but they displayed significantly longer hypocotyls than WT when grown in the light (SI Appendix, Fig. S3 A and B). To explore the genetic interactions between *SICPK27* and SIHY5, we generated double mutants of *slhy5 slcpk27* by crossing. While the *slhy5* mutants and *slcpk27* mutants developed longer hypocotyls than WT, *slhy5 slcpk27* double mutants showed a hypocotyl length similar to the *slcpk27* mutant in the light (Fig. 1H), indicating that *SICPK27* is epistatic to SIHY5.

To further examine the interplay between *SICPK27* and SIHY5, we performed transcriptomic analysis of WT, *slhy5*, and *slcpk27* seedlings grown in the W light for 4 d. The transcripts with ratios  $\geq 2$  or  $\leq 0.5$ , and *P*-values  $< 0.05$  were identified as differentially expressed genes (DEG). Based on this criterion, we identified 416 *SICPK27*-regulated DEGs and 890 SIHY5-regulated DEGs (SI Appendix, Dataset S1). Notably, 237 DEGs (56.97% of *SICPK27*-regulated DEGs and 26.6% of SIHY5-regulated DEGs) were co-regulated by *SICPK27* and SIHY5 (SI Appendix, Fig. S4A). Meanwhile, similar trends of changes in transcript levels of these co-regulated genes were observed in *slcpk27* and *slhy5* mutants (Fig. 1I and SI Appendix, Fig. S4B). Gene ontology (GO) analysis indicated that these genes were enriched in pathways related to “response to absence of light”, “cellular hormone metabolic process”, and “cytokinin metabolic process” (SI Appendix, Fig. S4C and SI Appendix, Dataset S2). Notably, “brassinosteroid (BR) homeostasis”, “BR biosynthetic process”, and “BR metabolic process” pathways were also highly enriched (SI Appendix, Fig. S4C and SI Appendix, Dataset S2), suggesting that *SICPK27* and SIHY5 co-regulate the expression of genes involved in BR homeostasis.

UPLC-MS/MS analysis demonstrated that the *slcpk27* mutants accumulated higher levels of 26-castasterone (CS, a precursor of BR) and brassinolide (BL, an active BR) than the WT (SI Appendix, Fig. S5 A and B). Meanwhile, *slcpk27* mutants had elevated transcript levels of *SIDWART* (*SIDWF*, a key gene in BR biosynthesis, encoding C-6 oxidase), while the transcripts of other key genes in BR biosynthesis, *SICPD*, *SIDET2*, and *SICYP90B3*, were not altered (SI Appendix, Fig. S5C). To determine whether the increased accumulation of BR contributed to the long hypocotyl phenotype of the *slcpk27* mutants, we compared the hypocotyl of *slcpk27* mutants with and without the application of brassinazole (BRZ, a specific inhibitor of BR biosynthesis). Results showed that there were no significant differences in the hypocotyl phenotype between WT and *slcpk27* mutants after the application of BRZ (SI Appendix, Fig. S5 D and E). Thus, *SICPK27* acts downstream of SIHY5 to regulate photomorphogenesis, potentially by modifying BR biosynthesis.

## **SICPK27 Interacts with and Phosphorylates SIPIF4 to Promote its Degradation**

To address the question of how SIHY5-regulated *SICPK27* inhibits hypocotyl elongation, we tried to identify the potential interaction partners of *SICPK27* by performing a yeast two-hybrid

(Y2H) screen. Among the 90 candidates (12), we focused on the basic helix–loop–helix (bHLH) transcription factor PIF4 as it is typically associated with light signaling pathways (13–16). Yeast-two hybrid assays demonstrated the interaction between *SICPK27* and SIPIF4 (Fig. 2A). Pull-down assay that used proteins with different tags purified from *Escherichia coli* further confirmed the direct interaction of *SICPK27* and SIPIF4 (Fig. 2B). We then performed bimolecular fluorescence complementation (BiFC) assay and observed strong YFP signals in the cells co-expressing SIPIF4-YN and *SICPK27*-YC, indicating that *SICPK27* physically interacts with SIPIF4 in vivo (Fig. 2C). The physical interactions were also confirmed by co-immunoprecipitation (co-IP) through transient overexpression of two proteins in *N. benthamiana*, and were further enhanced by  $\text{Ca}^{2+}$  treatment (Fig. 2D). Together, these results suggest that *SICPK27* physically interacts with SIPIF4 both in vitro and in vivo.

To investigate whether SIPIF4 is involved in *SICPK27*-mediated hypocotyl elongation, the accumulation of SIPIF4 protein in the *slcpk27* and WT seedlings was determined. While there were little differences in the accumulation of SIPIF4 protein in the WT and the *slcpk27* mutants in the dark, the *slcpk27* mutants had a much higher accumulation of SIPIF4 protein than WT in the light (Fig. 2E). Similarly, *slcpk27* mutants accumulated more SIPIF4 protein both in the nucleus and cytosol than the WT (Fig. 2F). Consistent with this, *SICPK27* protein showed both nuclear and cytoplasmic subcellular localization based on the transient overexpression of *SICPK27*-GFP in *N. benthamiana* (SI Appendix, Fig. S6 A and B). Although light promoted the accumulation of *SICPK27*-GFP, the allocation of *SICPK27* was not altered by light stimulus (SI Appendix, Fig. S6 C–E). Notably, light-induced degradation of SIPIF4 was inhibited by MG132, a 26S proteasome inhibitor, suggesting that *SICPK27* promoted the light-induced SIPIF4 degradation via the 26S proteasome pathway (Fig. 2G). Moreover, we found that  $\text{CaCl}_2$  promoted, while EGTA (a chelator of  $\text{Ca}^{2+}$ ) or  $\text{LaCl}_3$  (an inhibitor of  $\text{Ca}^{2+}$  channels) repressed light-induced SIPIF4 degradation (SI Appendix, Fig. S7). We then generated *slpif4* mutants in two tomato backgrounds (Condine Red and Alisa Craig, SI Appendix, Fig. S8A), and all the *slpif4* mutants displayed shorter hypocotyl phenotype compared with the WT (SI Appendix, Fig. S8B and Fig. 2H). To analyze the genetic link between *SICPK27* and SIPIF4, we generated *slcpk27 slpif4* double mutant by crossing *slcpk27* and *slpif4* mutants. In contrast with the long hypocotyl phenotype of *slcpk27* mutants, the *slcpk27 slpif4* double mutants showed a short hypocotyl phenotype (Fig. 2H), suggesting that increased accumulation of SIPIF4 in the *slcpk27* mutants contributes to its long hypocotyl phenotype.

Light-induced phosphorylation is a prerequisite for the degradation of PIFs protein (17). Considering that light triggers  $\text{Ca}^{2+}$  influx into the cytosol to promote plant photomorphogenesis (10), we first explored the effect of  $\text{Ca}^{2+}$  on light-induced phosphorylation of SIPIF4 using etiolated seedling. Light-induced SIPIF4 phosphorylation was found to be enhanced by  $\text{CaCl}_2$  treatment, but repressed by EGTA treatment and  $\text{LaCl}_3$  treatment compared with  $\text{H}_2\text{O}$  control (SI Appendix, Fig. S9A). Given that CPKs act as  $\text{Ca}^{2+}$  signal decoders, we then explored whether *SICPK27* directly phosphorylates SIPIF4 by performing Phos-tag mobility shift assays using purified His-*SICPK27* and MBP-SIPIF4 proteins from *E. coli* after in vitro phosphorylation reaction. The mobility shift band of MBP-SIPIF4 was observed in the presence of His-*SICPK27*, indicating that SIPIF4 was phosphorylated by *SICPK27* in vitro (Fig. 3A). When SIPIF4 and *SICPK27* were co-expressed in *N. benthamiana* leaves, phosphorylation of SIPIF4 was observed using an antibody that recognizes

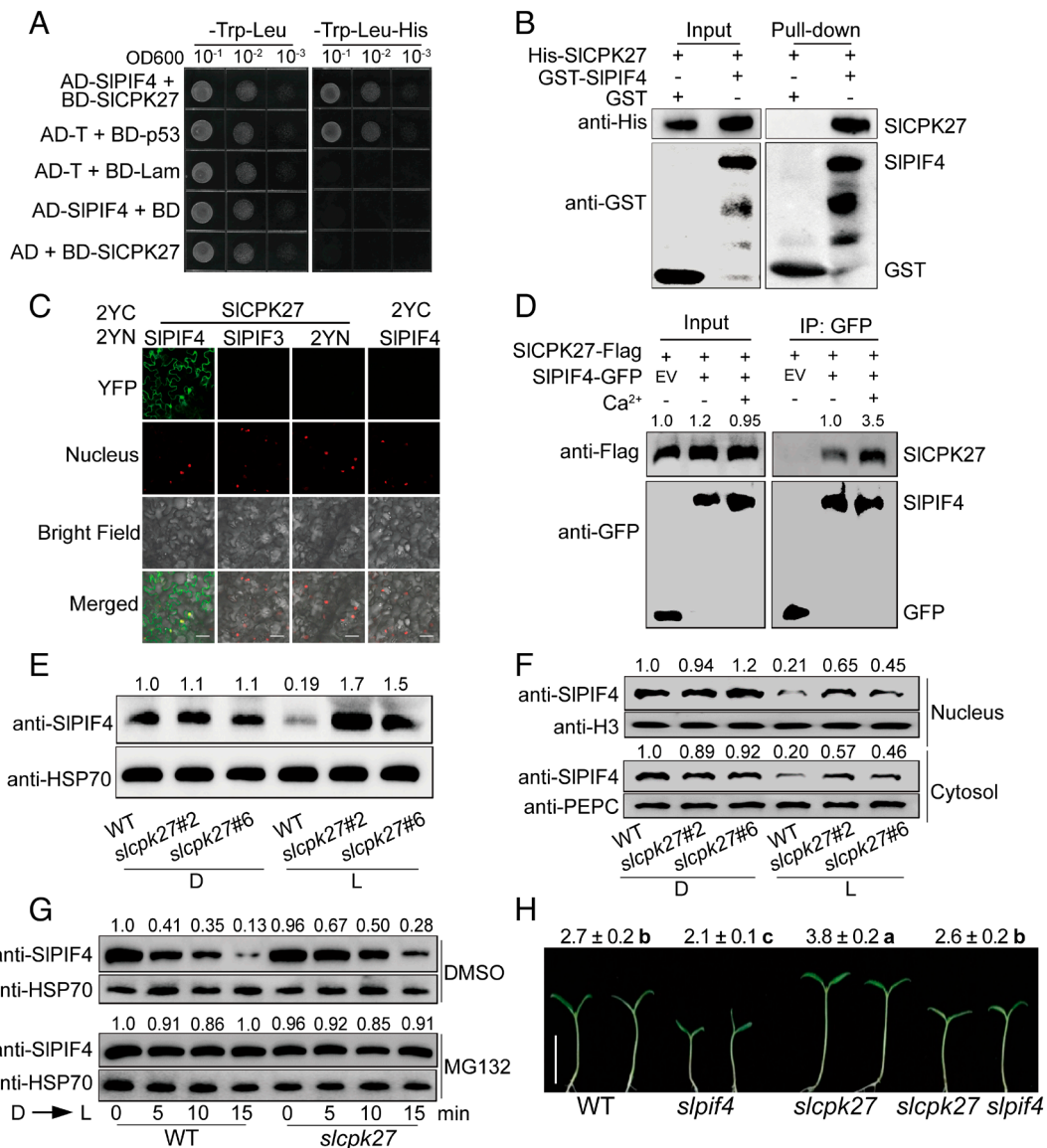


**Fig. 2.** SICPK27 interacts with SIPIF4 and promotes SIPIF4 protein degradation under light. (A) Y2H assay shows the interaction between SICPK27 and SIPIF4. Yeast growth on SD/-Trp, -Leu, -His solid medium is shown. AD-T and BD-p53 were used as the positive control, while AD-T and BD-Lam were used as negative control. (B) GST pull-down assay of the interaction between SICPK27 and SIPIF4 in vitro. GST or GST-SIPIF4 fusion proteins coupled with glutathione beads were used to pull down His-SICPK27. (C) BiFC assay showing the interaction of SICPK27 with SIPIF4, but not SIPIF3 in *N. benthamiana* leaves. Images were taken using a confocal microscope. Bar = 25  $\mu$ m. (D) Co-IP assays showing the interaction of SICPK27 with SIPIF4 in *N. benthamiana* leaves. CaCl<sub>2</sub> was supplied at 15 mM. The relative levels of SICPK27-Flag, normalized to GFP or SIPIF4-GFP, were shown above the SICPK27-Flag immunoblots. (E) Immunoblots showing total SIPIF4 protein levels in 4-d-old WT and *slcpk27* mutant seedlings grown in continuous dark (D) or white light (L). The relative levels of SIPIF4, normalized to HSP70, were shown above the SIPIF4 immunoblots. (F) SIPIF4 protein levels in the nucleus and cytosol of 4-d-old WT and *slcpk27* mutant seedlings grown in the continuous dark (D) or white light (L). The relative levels of SIPIF4, normalized to PEPC or H3, were shown above the SIPIF4 immunoblots. (G) Immunoblots showing SIPIF4 protein levels in 4-d-old etiolated WT and *slcpk27* mutant seedlings transferred to white light for the indicated periods in the presence of MG132 or DMSO. The relative levels of SIPIF4, normalized to HSP70, were shown above the SIPIF4 immunoblots. (H) Hypocotyl phenotypes of 4-d-old WT (Condine Red), *slpif4*, *slcpk27*, and *slpif4 slcpk27* seedlings grown in continuous white light. Bar = 2 cm. The hypocotyl lengths above the graph are shown as mean  $\pm$  SD ( $n \geq 20$ ). Different letters indicate significant differences according to Tukey's test ( $P < 0.05$ ).

the phosphorylated serine and threonine residues (anti-pSer/pThr). This phosphorylation was further promoted by Ca<sup>2+</sup> and light stimuli (Fig. 3B and C). By using *N. benthamiana* leaves overexpressing GFP-tagged SICPK27, we found that Ca<sup>2+</sup> increased, while EGTA or LaCl<sub>3</sub> decreased the SICPK27-GFP phosphorylation level and kinase activity as indicated by MBP-SIPIF4 phosphorylation levels (Fig. 3D). Meanwhile, immunoblotting with an anti-pSer/pThr antibody demonstrated that the SICPK27-GFP phosphorylation level and kinase activity increased as soon as 5 min after exposure to light (Fig. 3E). These data collectively revealed that SICPK27 phosphorylates SIPIF4 in a Ca<sup>2+</sup>- and light-dependent manner.

By LC-MS/MS analysis, we identified two phosphosites, serine-252 (Ser-252) and serine-308 (Ser-308), in the SIPIF4 protein (Fig. 3F). Notably, Ser-308 was located in the bHLH domain of the SIPIF4 protein (SI Appendix, Fig. S9B). Interestingly, these two sites are highly conserved in PIF4 putative homologs in potato (*Solanum tuberosum*, Soltu.DM.07G014300.2), pepper (*Capsicum annuum*, XP\_016580439.1), tobacco (*Nicotiana tabacum*, XP\_016471316.1), and *Arabidopsis* (AT2G43010.5) (SI Appendix, Fig. S9C), implying that these phosphorylation events might also occur in other plant species. To verify the role of these identified phosphorylation sites, we mutated the substituted serine (S) residues to alanine (A) to mimic the dephosphorylation status. By transiently overexpressing

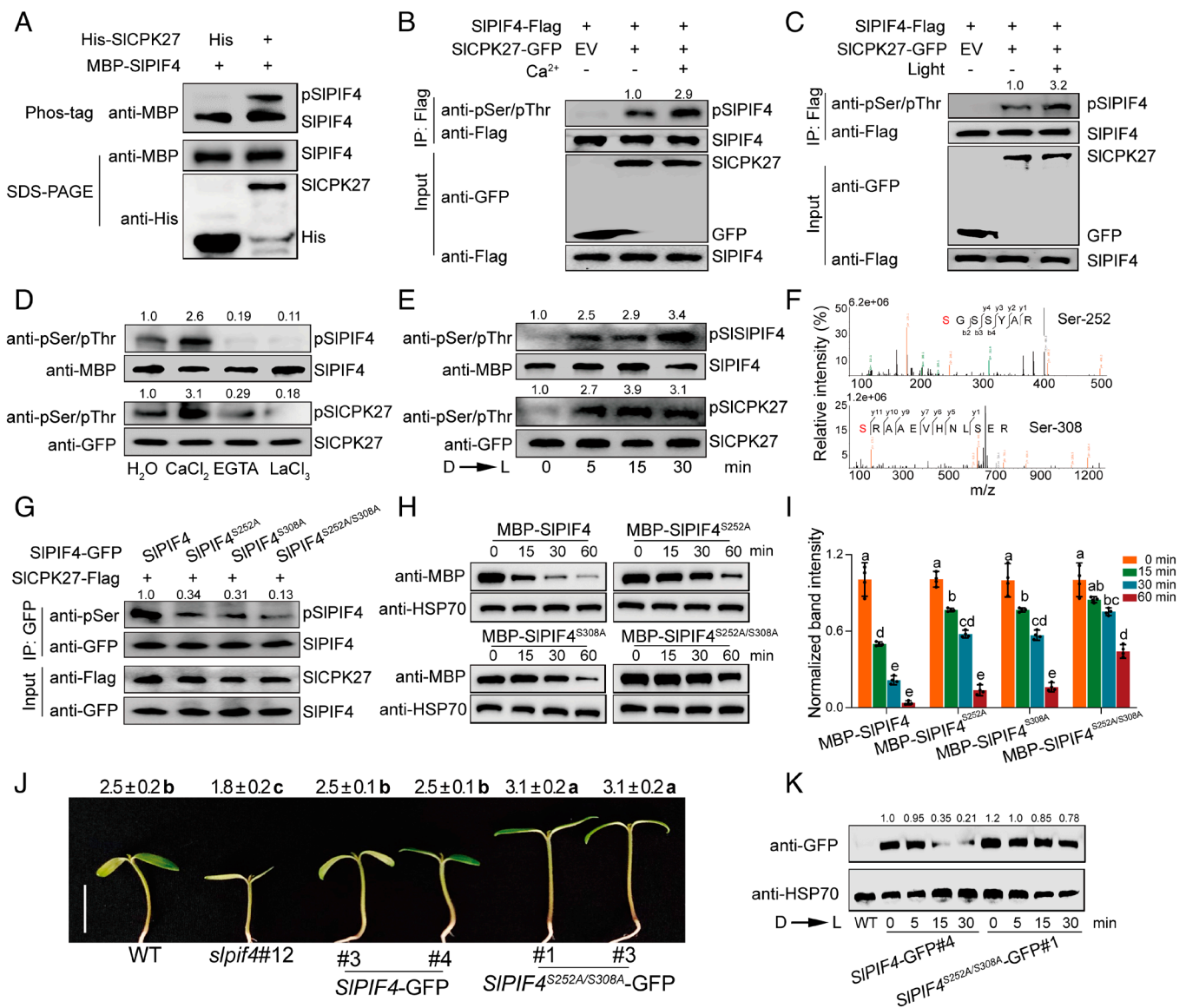


**Fig. 3.** Phosphorylation of SIPIF4 by SICPK27 contributes to light-induced SIPIF4 protein degradation. (A) SICPK27 phosphorylates SIPIF4 in vitro. The phosphorylated SIPIF4 protein was detected by Phos-tag SDS-PAGE assay. (B) Ca<sup>2+</sup> promotes SICPK27-mediated phosphorylation of SIPIF4 in *N. benthamiana* leaves. CaCl<sub>2</sub> was supplied at 15 mM. The relative phosphorylation levels of pSIPIF4, normalized to IP SIPIF4-Flag, were shown above the pSIPIF4 immunoblots. (C) Light promotes SICPK27-mediated phosphorylation of SIPIF4 in *N. benthamiana* leaves which were kept in the dark or transferred to light for 2 h before sampling. The relative phosphorylation levels of pSIPIF4, normalized to IP SIPIF4-Flag, were shown above the pSIPIF4 immunoblots. (D) Ca<sup>2+</sup> and (E) light increase the phosphorylation level and kinase activity of SICPK27. The *N. benthamiana* leaves transiently overexpressing SICPK27-GFP were kept in the darkness (D) and transferred to light (L) for the indicated time or subjected to pharmacological treatments. The relative phosphorylation levels of pSICPK27 and pSIPIF4, normalized to SICPK27-GFP or MBP-SIPIF4 respectively, were shown above the pSICPK27 and pSIPIF4 immunoblots. (F) LC-MS/MS analysis revealed that Ser-252 and Ser-308 sites of SIPIF4 are phosphorylated by SICPK27. (G) Site-directed mutation of Ser residues in SIPIF4 inhibited its phosphorylation by SICPK27. The relative phosphorylation levels of pSIPIF4, normalized to IP SIPIF4-Flag, were shown above the pSIPIF4 immunoblots. (H) Degradation of MBP-SIPIF4 and its mutant form in cell-free assays from WT protein extracts. (I) Quantification of MBP-SIPIF4 protein band in (H). The protein abundance of MBP-SIPIF4 in 0 min of each treatment was defined as 1. Data are shown as mean ± SD (*n* = 4). (J) Hypocotyl phenotypes of 4-d-old WT (*Ailsa Craig*), *slpif4#12*, *proSIPIF4: SIPIF4-GFP* (*SIPIF4-GFP*), *proSIPIF4: SIPIF4<sup>S252A/S308A</sup>-GFP* (*SIPIF4<sup>S252A/S308A</sup>-GFP*) seedlings grown under continuous white light. Bar = 2 cm. The hypocotyl lengths above the graph are shown as mean ± SD (*n* ≥ 20). (K) Immunoblots showing SIPIF4 protein levels in seedlings transferred from dark (D) to white light (L) for the indicated periods. The relative levels of SIPIF4-GFP, normalized to HSP70, were shown above the SIPIF4-GFP immunoblots. In (I) and (J), different letters present significant differences according to ANOVA followed by Tukey's test (*P* < 0.05).

SICPK27-Flag and SIPIF4-GFP in *N. benthamiana*, we found that mutations of these sites substantially attenuated SICPK27-mediated phosphorylation of SIPIF4 (Fig. 3G), supporting that Ser-252 and Ser-308 in the SIPIF4 are phosphorylated by SICPK27 kinase in vivo. However, no significant differences in subcellular location, interaction with SICPK27, transcriptional activity, or binding ability were observed between SIPIF4 and its mutant forms (SI Appendix, Fig. S10 A–D). Importantly, recombinant mutagenized protein, especially MBP-SIPIF4<sup>S252A/S308A</sup>, showed lower degradation rates than MBP-SIPIF4 protein in a cell-free system (Fig. 3H and I), indicating

that the stability of SIPIF4 was under the control of SICPK27-mediated phosphorylation.

We then examined the physiological significance of the SICPK27-mediated phosphorylation of SIPIF4 in regulating photomorphogenesis by generating native promoter-driven stable genetically complementary *SIPIF4-GFP* and *SIPIF4<sup>S252A/S308A</sup>-GFP* lines in the *slpif4* mutant background (SI Appendix, Fig. S11A). The transgenic lines with similar expression levels of *SIPIF4* and *SICPK27* were used (SI Appendix, Fig. S11 B and C). Consistently, *SIPIF4<sup>S252A/S308A</sup>-GFP* lines exhibited an elongated hypocotyl

phenotype compared with WT, whereas *SIPIF4*-GFP lines only restored the photomorphogenic defects of the *slpif4* mutant (Fig. 3*f*). Moreover, mutation of *SIPIF4* phosphosites did not alter its protein levels in dark-grown seedlings but largely abolished the light-triggered degradation of *SIPIF4* during the dark-to-light transition (Fig. 3*k*). Confocal GFP fluorescence also showed that a higher level of *SIPIF4* protein was accumulated in *SIPIF4*<sup>S252A/S308A</sup> lines (SI Appendix, Fig. S11 D and E). Therefore, SICPK27-mediated phosphorylation of *SIPIF4* is essential for its degradation in response to light.

## SIPIF4 Regulates BR Biosynthesis to Promote Hypocotyl Elongation

Auxin and BR play a crucial role in the PIF4-regulated hypocotyl elongation (5, 18–20). Recent results from several studies suggest that auxin function is strictly dependent on BR (21, 22). Here, we found that *slpif4* mutants showed significantly reduced contents of CS, BL, and indole-3-acetic acid (IAA) relative to WT under light conditions (Fig. 4 A–C). We subsequently tried to

differentiate the role of BR from auxin in the *SIPIF4*-regulated hypocotyl elongation by exogenous application 24-epibrassinolide (eBL) and synthetic auxin picloram (Pic). eBL significantly promoted hypocotyl elongation of WT and rescued the short hypocotyl phenotype of *slpif4* mutants (SI Appendix, Fig. S12 A and B). In contrast, Pic only partially rescued the hypocotyl defective phenotype of *slpif4* (SI Appendix, Fig. S12 C and D), suggesting that BR plays a predominant role in *SIPIF4*-mediated hypocotyl elongation.

RT-qPCR analysis revealed that the transcript accumulation of *SIDWF* was decreased in *slpif4* mutants but no significant changes in the transcript accumulation of other BR biosynthesis genes were observed as compared with WT (Fig. 4D and SI Appendix, Fig. S13). To test whether *SIPIF4* directly regulates *SIDWF* expression, we performed EMSA and found that MBP-*SIPIF4* could bind the promoter of *SIDWF* at all G-box-like motifs (Fig. 4E). ChIP assays using light-grown *SIPIF4*-GFP seedlings further confirmed the binding of *SIPIF4* to the *SIDWF* promoter in vivo (Fig. 4F). LUC assays showed that the expression of *LUC* driven by *SIDWF* promoter was higher in *N. benthamiana* leaves that expressed

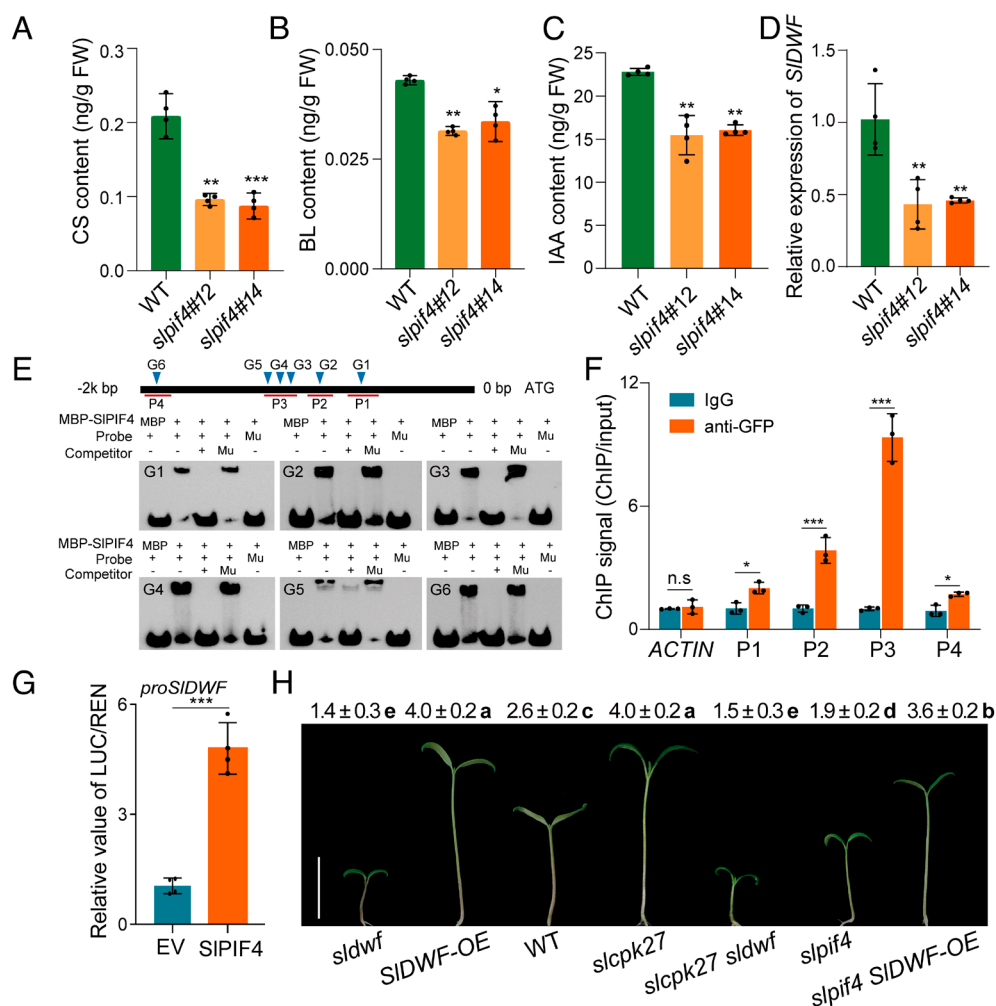


**Fig. 4.** *SIPIF4* negatively regulates photomorphogenesis by triggering BR biosynthesis. Content of (A) 26-castasterone (CS), (B) brassinolide (BL), and (C) indole-3-acetic acid (IAA) in 4-d-old WT (*Ailsa Craig*) and *slpif4* seedlings grown in continuous white light. (D) Expression of *SIDWF*, a BR biosynthesis gene, of seedlings in (A). (E) Diagram of *SIDWF* promoter region and EMSAs showing the binding ability of *SIPIF4* to the *SIDWF* promoter. The blue deltas represent potential *SIPIF4* binding sites (G-Box-like motifs). P1, P2, P3, and P4 indicate the promoter fragments identified by ChIP-qPCR. Competitors and mutant competitors were used at 100-fold. Mu, mutated probe in which the CACATG motif was changed to AAAAAA. (F) ChIP-qPCR analysis showing the binding ability of *SIPIF4* to the *SIDWF* promoters. (G) Dual-luciferase assays for the regulatory effect of *SIPIF4* on the expression of *SIDWF*. The ratio of LUC/REN of the EV (empty vector) was set as 1. (H) Hypocotyl phenotypes of 4-d-old *sldwf*, *SIDWF-OE*, WT (*Condine Red*), *slcpk27*, *slcpk27 sldwf*, *slpif4*, and *slpif4 DWF-OE* seedlings grown under white light. Bar = 2 cm. The hypocotyl lengths above the graph are shown as mean ± SD ( $n \geq 20$ ). Data are shown as mean ± SD,  $n = 4$  in (A–D) and (G), and  $n = 3$  in (F). Different letters present significant differences according to ANOVA followed by Tukey's test ( $P < 0.05$ ) and asterisks present significant differences compared with WT or indicated control according to Student's *t* test (\* $P < 0.05$ , \*\*\* $P < 0.01$ ).

SIPIF4-Flag than empty vector control (Fig. 4G). Collectively, these results demonstrate that SIPIF4 acts as the transcriptional activator of *SIDWF*. Consistent with the role of BR in the photomorphogenesis (23), *sl dwarf* mutants showed shorter hypocotyl while *SIDWF*-over expressing (*SIDWF*-OE) lines showed longer hypocotyls. Importantly, mutation of *SIDWF* in *slcpk27* mutant (*slcpk27 sl dwarf*) compromised the long hypocotyl phenotype of *slcpk27* while *SIDWF*-over expression in *slpif4* rescued the short hypocotyl phenotype of *slpif4* (Fig. 4H). In agreement with the crucial role of BR in hypocotyl elongation, changes in hypocotyl phenotype were not consistent with the changes in IAA accumulation and transcript of auxin biosynthesis gene *SIYUC8* and signaling gene *SILAA19* in the seedlings (SI Appendix, Fig. S14 A–C). Collectively, these data strongly suggest that SIPIF4 plays a crucial role in hypocotyl elongation mainly by activating BR biosynthesis.

## SIHY5-SICPK27-SIPIF4-BR Module Plays a Role in Thermomorphogenesis

Besides light, temperature is also a key environment cue regulating plant growth and development. phyB is known to possess the ability to sense light and temperature cues to coordinate hypocotyl elongation (6, 24, 25). To determine whether the SIHY5-SICPK27-SIPIF4 module also participates in the regulation of thermomorphogenesis, we incubated photoreceptor mutants (*slphyA*, *slphyB1B2*, *slphyAB1B2*, and *slcry1a*) in the light at 25 °C or 32 °C. While warm temperature significantly induced hypocotyl elongation in WT, this increase was attenuated in *slphyA*, *slphyB1B2*, and *slcry1a* and abolished in *slphyAB1B2* (Fig. 5 A and B). In addition, warm temperatures decreased the accumulation of SIHY5 protein but increased the accumulation of SIPIF4 protein in WT seedlings (Fig. 5C). These changes, however, were again attenuated in the photoreceptor mutants, especially in *slphyB1B2*, and *slphyAB1B2* mutants (Fig. 5C). While warm temperature significantly decreased the transcript of *SICPK27* and increased the transcript of *SIDWF* in WT seedlings, respectively, these changes were attenuated in these photoreceptor mutants, especially in *slphyB1B2*, and *slphyAB1B2* mutants (Fig. 5 D and E). Therefore, *SlphyA*, *SlphyB*, and *SlCRY1A* are all involved in the regulation of thermomorphogenesis with *SlphyB* playing a crucial role.

We then determined the role of *SIHY5*, *SICPK27*, *SIPIF4*, and *SIDWF* in thermomorphogenesis. While an increase in ambient temperature induced an increase in hypocotyl lengths by 60.4% in WT, it had marginal effects on the hypocotyl lengths in *slhy5* and *slcpk27* mutants and no significant effects in *slpif4* and *sl dwarf* mutants (Fig. 5 F and G). Consistent with the hypocotyl phenotype, warm temperature induced minor changes in the SIPIF4 protein accumulation in *slhy5* and *slcpk27* mutants while that in *sl dwarf* was not different from WT (Fig. 5H). Meanwhile, warm temperature significantly reduced the *SICPK27* expression in WT seedlings but not in *slhy5* mutant (Fig. 5I). While an increase in the ambient temperature resulted in about a 2.6-fold increase in the *SIDWF* expression in WT seedlings, this increase was diminished in *slhy5* and *slcpk27* mutants and completely abolished in the *slpif4* mutant (Fig. 5J). To verify the role of BR in thermomorphogenesis, we incubated the WT, *slhy5*, *slcpk27*, and *slpif4* seedlings at 25 °C or 32 °C in the presence of BRZ or not. As shown in SI Appendix Fig. S15, an increased-ambient-temperature substantially induced hypocotyl elongation in WT. In contrast, the hypocotyl elongation was less pronounced in the *slhy5* and *slcpk27* mutants. These effects were, however, eliminated by BRZ. Collectively, these results highlight the essential role of the SIHY5-SICPK27-SIPIF4 module in thermomorphogenesis by regulating BR biosynthesis.

## Discussion

Light is a critical environmental cue that triggers cytosolic  $\text{Ca}^{2+}$  influx in plants (8, 26, 27).  $\text{Ca}^{2+}$ , as a universal intracellular second messenger, can promote light-responsive gene expression in tomato hypocotyl cells (9). Although the involvement of  $\text{Ca}^{2+}$  in light signaling was discovered decades ago, the molecular mechanism of how plants convert light-induced  $\text{Ca}^{2+}$  signals into downstream events has been a long-standing puzzle. A recent study showed that phyB-mediated  $\text{Ca}^{2+}$  signal can be sensed by CPK6/12, which in turn phosphorylates phyB to promote its nuclear import in *Arabidopsis* (10). Unlike the way phyB directly induces cytosolic  $\text{Ca}^{2+}$  level (10), here we found that the SIHY5 promotes the expression of a  $\text{Ca}^{2+}$  signal decoder, *SICPK27* (Fig. 1 C–G). *SICPK27* subsequently transmits the  $\text{Ca}^{2+}$  signal by phosphorylating SIPIF4 to repress its accumulation (Fig. 3). Therefore, data in this study present critical evidence that light and  $\text{Ca}^{2+}$  signals are tightly integrated during tomato photomorphogenesis.

PIFs act as central signaling hubs that coordinate plant growth in response to a wide range of environmental cues. Light-induced PIF phosphorylation is vital for its degradation and several kinases can promote the degradation by phosphorylation of PIF1/3 (6, 28–30), but light-responsive kinases with PIF4 phosphorylation ability are still needed to be investigated. It was once widely believed that phyB can phosphorylate PIF4 in response to light for its degradation through the 26S proteasome system (6), structure analysis, however, revealed that phyB is probably not a protein kinase (31). In this regard, the findings in this study uncover that SIHY5-promoted *SICPK27* directly phosphorylates SIPIF4 to facilitate its degradation in the light (Fig. 3), demonstrating an important and previously unrecognized role of *SICPK27* in the SIHY5- and SIPIF4-dependent photomorphogenesis. Notably, the BR signaling pathway component, BIN2, was found to phosphorylate and mediate the degradation of PIF4 (13). Considering that PIF4 mediates both BR and light signals in a phosphorylation-dependent manner, a fundamental question of how PIF4 distinguishes the particular signaling pathway then arises. *SICPK27* phosphorylates SIPIF4 at Ser-252 and Ser-308 (Fig. 3F), which is different from the BIN2-mediated phosphosites (13), indicating that diverse phosphosites are associated with different signaling pathways. Therefore, this phosphocode-based regulation of PIF4 by different protein kinases is important for its biological function in response to different environmental stimuli.

BR and auxin are two major phytohormones thought to be involved in the PIF4-regulated hypocotyl elongation (5, 18, 21, 32). While mutations in *SIPIF4* resulted in a decrease in BR and IAA, genetic complement and pharmacological experiments as well as the inconsistency of IAA accumulation with hypocotyl phenotype all demonstrated that BR dominates the hypocotyl elongation relative to auxin (Fig. 4H and SI Appendix, Figs. S12 and S14). This is in agreement with a previous study showing that hypocotyl defects of both BR biosynthesis and signaling mutants could not be rescued by exogenous auxin, while exogenous BR rescued hypocotyl defects in auxin biosynthesis and signaling mutants during thermomorphogenesis in *Arabidopsis* (21). Most recently, the role of BR in hypocotyl elongation has been underscored again by the findings that green light-induced hypocotyl elongation is primarily dependent on BR rather than auxin (33).

Exposure to light is typically concomitant with a temperature rise, therefore, a large set of common signaling components are usually shared in light and temperature signal pathways (34). While the photoreceptors directly interact with PIF4, here we demonstrated that the photoreceptor-regulated SIHY5-SICPK27-SIPIF4-BR module not only plays a vital role in photomorphogenesis

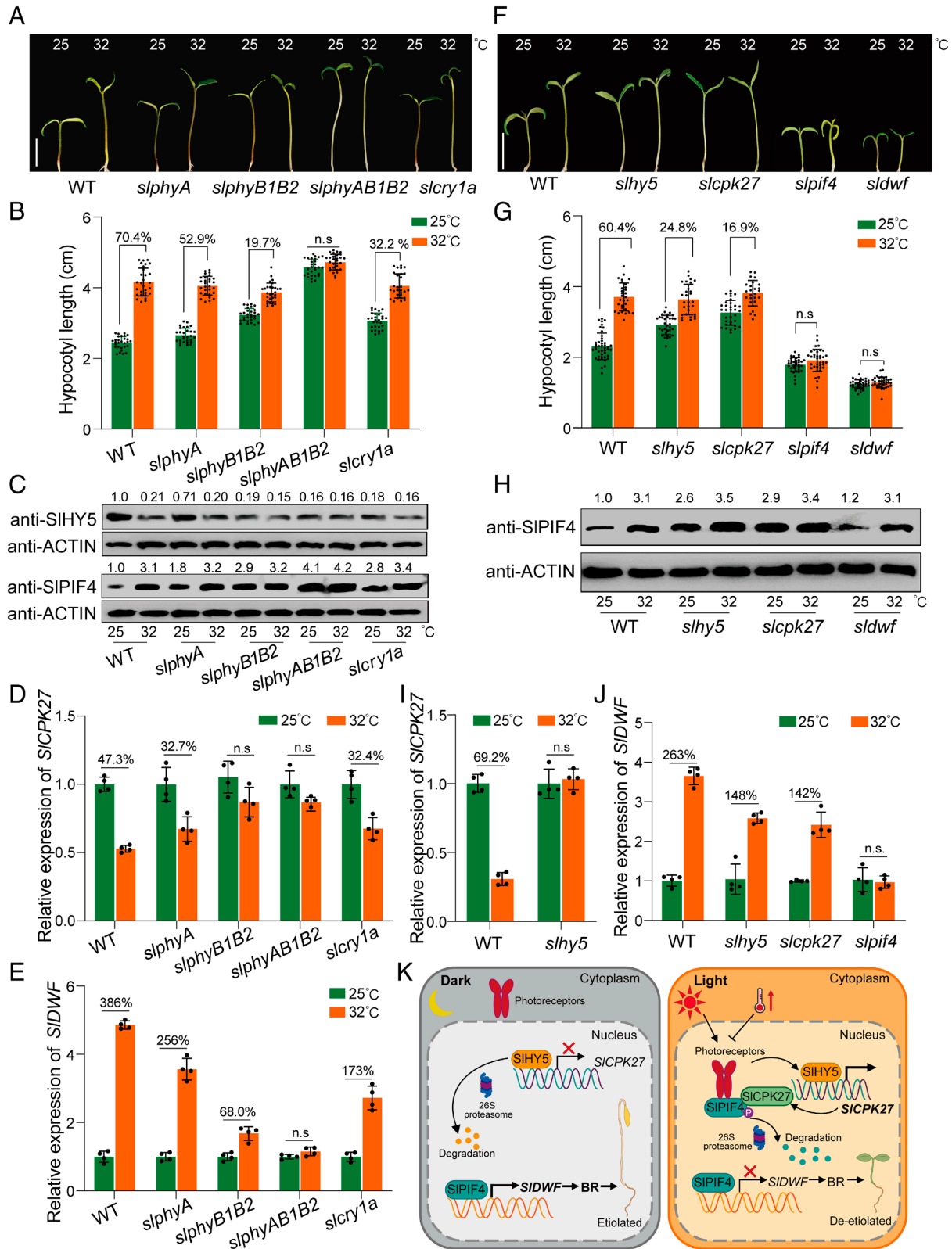


**Fig. 5.** SIHY5-SICPK27-SIPIF4-BR module is involved in tomato thermomorphogenesis. (A) Hypocotyl phenotypes and (B) hypocotyl lengths of 4-d-old WT, *sphyA*, *sphyB1B2*, *sphyAB1B2*, and *slcry1a* seedlings. Bar = 2 cm. (C) Immunoblots showing SIHY5 and SIPIF4 protein levels in seedlings in (A). The relative levels of SIHY5 and SIPIF4, normalized to ACTIN, were shown above the SIHY5 and SIPIF4 immunoblots. (D) Expression of *SICPK27*, and (E) *SIDWF* of seedlings in (A). (F) Hypocotyl phenotypes and (G) hypocotyl lengths of 4-d-old WT (Condine Red), *slhy5*, *slcpk27*, *slpif4*, and *sldwf* seedlings. Bar = 2 cm. (H) Immunoblots showing SIPIF4 protein levels of seedlings in (F). The relative levels of SIPIF4, normalized to ACTIN, were shown above the SIPIF4 immunoblots. (I) Expression of *SICPK27* in 4-d-old WT (Condine Red), and *slhy5* seedlings and (J) expression of *SIDWF* in 4-d-old WT (Condine Red), *slhy5*, *slcpk27*, and *slpif4* seedlings. Relative expression of *SICPK27* and *SIDWF* were calculated against the expression level in the 25 °C of each genotype, which was designated as 1. Data are shown as mean  $\pm$  SD,  $n \geq 25$  in (B) and (G),  $n = 4$  in (D), (E), (I), and (J). The Student's t test ( $P < 0.05$ ) was used to compare significant differences between 32 °C and 25 °C. n.s., not significant. (K) Working model depicting the roles of SICPK27 in regulating photomorphogenic and thermomorphogenic development.

but also essentially functions in the correct thermal sensing in the hypocotyl elongation (Fig. 5K). The hypocotyl elongation of photoreceptor mutants, *slhy5*, *slcpk27*, *slpif4*, and *sldwf* mutants was negligible compared with WT in response to the increase in growth temperature (Fig. 5 A and F). Consistent with this, in *Arabidopsis*, the key light signaling components, including photoreceptors, COP1, HY5, and PIF4, have also been identified as regulators of the thermal sensing system (24, 32, 35–39). This multipurpose signaling module indicates potential co-evolution of light and temperature signal transduction, which grants plants greater flexibility to fine-tune their physiological processes to better adapt to the dynamic fluctuations in their environment.

## Materials and Methods

**Plant Materials and Growth Conditions.** Wild-type tomato (*Solanum lycopersicum*) cv. Moneymaker; cv. Condine Red; cv. Ailsa Craig; and the *slphyA*, *slphyB1B2*, *slphyAB1B2*, *slcry1a*, and *sldwf* mutants were obtained from the Tomato Genetics Resource Center at the University of California, Davis (<http://tgrc.ucdavis.edu>). The CRISPR/Cas9 mutants of *slhy5#1* and *SIHY5-OE* transgenic plants in the cv. Ailsa Craig background, and *slhy5* mutant in cv. Condine Red backgrounds were generated as described previously (40, 41). The *SIDWF-OE* line was generated as previously reported (23). The CRISPR/Cas9 mutants of *slpif4* and *slcpk27* (*slcpk27#2*, *slcpk27 #6* lines) in the cv. Condine Red background and *slpif4* (*slpif4#12*, *slpif4#14* lines) in the cv. Ailsa Craig background were generated similarly to previous studies (41). The complementary lines of *proSIPIF4*: *SIPIF4*-GFP and *proSIPIF4*: *SIPIF4*<sup>S252A/S308A</sup>-GFP were generated in the *slpif4#12* mutant background. The double-mutant *slhy5 slcpk27*, *slcpk27 sldwf*, *slcpk27 slpif4*, *slpif4 SIDWF-OE* was generated by crossing, and the homozygous F3 generation was used.

Tomato seeds were surface sterilized with 75% (v/v) ethanol for 30 s followed by 15 min in 10% (v/v) NaClO. Germinated seeds were incubated for 4 d on half-strength Murashige and Skoog (1/2 MS) media (Solarbio, M8526, China) supplemented with 0.8% (w/v) agar and 1% sucrose under different temperatures in the dark or in the light conditions (white light, 380 to 780 nm, 200  $\mu\text{mol m}^{-2} \text{s}^{-1}$ ; blue light, 400 to 500 nm, 200  $\mu\text{mol m}^{-2} \text{s}^{-1}$ ; red light, 600 to 700 nm, 200  $\mu\text{mol m}^{-2} \text{s}^{-1}$ ; far-red light, 700 to 750 nm, 200  $\mu\text{mol m}^{-2} \text{s}^{-1}$ ). Then, hypocotyl lengths were measured using ImageJ software.

**RNA Extraction and RT-qPCR.** Total RNA was extracted from 4-d-old tomato seedlings using FastPure Universal Plant Total RNA Isolation Kit (Vazyme Biotech Co. Ltd, RC411-01, China). Total RNA (0.5  $\mu\text{g}$ ) was reverse transcribed into cDNA using the Evo M-MLV Mix Kit with gDNA Clean for qPCR (Accurate Biology, AG11728, China) according to the manufacturer's instructions. The RT-qPCR analysis was performed using Hieff<sup>®</sup> qPCR SYBR Green Master Mix (11201, Yeasen, Shanghai, China) and conducted on the Light Cycler<sup>®</sup> 480 II Real-Time PCR Detection System (Roche, Swiss). The PCR was performed for 3 min at 95 °C, followed by 45 cycles of 95 °C for 10 s, 57 °C for 15 s, and 72 °C for 10 s. The tomato housekeeping gene *ACT1N* was used as an internal control to calculate the relative expression of target genes. Sequences of primers are listed in *SI Appendix, Table S1*.

**RNA Transcriptome Analyses.** Total RNA was extracted from the 4-d-old WT, *slhy5*, and *slcpk27* seedlings grown in constant white light (200  $\mu\text{mol m}^{-2} \text{s}^{-1}$ ) conditions. mRNA sequencing libraries were constructed, and sequencing was performed using the Illumina HiSeq 2500 platform according to the manufacturer's instruction by the Shanghai Bioprofile Technology Company Ltd. The cleaned reads were aligned to the tomato genome sequence SL4.00 (Sol Genomics Network) by the Hierarchical Indexing for Spliced Alignment of Transcripts (HISAT) software (version 0.1.6), allowing one mismatch to generate unique sequences. Three independent biological replicates were performed in which the WT, *hy5*, and *cpk27* were sampled independently. To identify DEGs (differential expression genes) between different groups, the expression level of each transcript was calculated according to the transcripts per million reads (TPM) method. The transcripts with ratios  $\geq 2$  or  $\leq 0.5$ , and *P*-values (false discovery rate, FDR)  $< 0.05$  were identified as DEGs. GO analysis was performed using Shiny GO (42), and the results were plotted using ggplot2 with R (43).

**Measurement of Phytohormones.** The phytohormone measurement procedure followed previously published methods (23). To quantify BR, 0.1 g of the sample underwent grinding into a fine powder and was then combined with 1 mL of ice-cold acetonitrile. Internal standards, specifically (<sup>2</sup>H<sub>3</sub>) castasterone (D-CS) and (<sup>2</sup>H<sub>3</sub>) brassinolide (D-BL) sourced from Olchemim, Olomouc, Czech Republic, were incorporated into the extraction solution. Following an overnight extraction period at 4 °C and subsequent centrifugation at 10,000 g for 10 min at 4 °C, the supernatant was collected and transferred into a 10 mL tube. In this tube, 0.3 g of 2-(4-boronobenzyl) isoquinolin-2-ium-modified MCX material and 3 mL of ddH<sub>2</sub>O were added. After stirring for 5 min and centrifugation at 10,000 g for 1 min at 4 °C, the resulting pellet was resuspended in 5 mL of 90% (v/v) acetone with the addition of 0.5% (v/v) formic acid. Subsequent steps included the addition of 1.2 mL of 90% (v/v) acetone and 50 mg of CH<sub>3</sub>COONH<sub>4</sub>, followed by stirring for 1 min and centrifugation at 10,000 g for 3 min. The upper phase was then collected and evaporated to dryness using N<sub>2</sub> flow. The resulting sample residue was resuspended in 100  $\mu\text{L}$  of 45% (v/v) acetonitrile and transferred into analysis tubes. For the quantification of indole-3-acetic acid (IAA), 0.1 g of 4-d-old seedlings was ground into a powder using liquid nitrogen and homogenized in 1 mL of ethyl acetate spiked with D6-IAA, serving as internal standards. The mixture was then shaken at 180 rpm in the dark at 4 °C for 12 h and subsequently centrifuged at 12,000 g for 15 min at 4 °C. The resulting pellet underwent re-extraction with 1 mL of ethyl acetate. The supernatants were evaporated to dryness under N<sub>2</sub> flow. The residue was then resuspended in 500  $\mu\text{L}$  of 70% methanol (v/v) and centrifuged, with 200  $\mu\text{L}$  of the solution transferred to UPLC/MS analysis tubes. All extracted samples were analyzed utilizing ACQUITY UPLC<sup>®</sup>-I-Class coupled to a Waters XevoTM TQ-XS triple quadrupole mass spectrometer.

**Protein Extraction and Western Blot.** Protein extraction and immunoblotting were performed according to a previous study (20) with minor modifications. Briefly, about 0.1 g 4-d-old seedlings were ground to a fine powder in liquid nitrogen and then transferred to 0.2 to 0.3 mL extraction buffer (50 mM Tris-HCl, pH 7.5, 10 mM EDTA, pH 8.0, 150 mM NaCl, 50 mM dithiothreitol, 1% Triton X-100, 1 mM phenylmethylsulfonyl fluoride, 0.2%  $\beta$ -mercaptoethanol, and protease inhibitor cocktail). The extracts were mixed fully and incubated on ice for 15 min, followed by centrifugation at 13,000 g for 20 min at 4 °C, after which the extracted proteins were denatured at 95 °C for 10 min. Then, these samples were separated by SDS-PAGE, in which the gels were made using the One-Step Colored PAGE Gel Fast Preparation Kit (SKV-0055, Share-bio, Shang Hai), and transferred to nitrocellulose membranes (Millipore, France). The SIHY5 and SIPIF4 protein was detected with anti-SIHY5 and anti-SIPIF4 antibodies respectively, which were produced by Shanghai Jiayuan Bio Co. Ltd. (Shanghai, China). Targeted proteins were visualized using the EZ ECL pico luminescence reagent (AP34L024, Life-iLab, China). The SICPK27-Flag, SIPIF4-Flag, SICPK27-GFP, SIPIF4-GFP, MBP-SIPIF4, GST-SIPIF4, His-SICPK27 proteins were detected with commercial antibodies (anti-Flag, Sigma-Aldrich, A8592; anti-GFP, Thermo-Fisher, MA5-15256; anti-MBP, Beijing Ray, RM1007; anti-GST, Beijing Ray, RM1005; anti-His, share-bio, Shang Hai, SB-AB0002). Actin (anti-Actin, ABclonal, A23959) and HSP70 (anti-HSP70, ABclonal, A12948) were used as loading controls.

**Recombinant Protein Purification and EMSA.** The pET-32a-His-SIHY5 vector was constructed as described previously (41). The full-length SICPK27 and SIPIF4 CDS were amplified from cDNA using *TransStart<sup>®</sup> FastPfu* DNA Polymerase (AP221, TransGen Biotech, China) with the gene-specific primers listed in *SI Appendix, Table S2*. Purified PCR products were cloned into pET-32a and pMal-c2x vectors respectively, using the Spark DNA Quick Ligation Kit (AK0901, Shandong Sparkjade Biotechnology Co., Ltd.). The recombinant vectors were transformed into *Escherichia coli* strain BL21 (DE3). The His-SIHY5, His-SICPK27, and MBP-SIPIF4 recombinant proteins were separately expressed and purified Ni-NTA Agarose (Qiagen, Germany), or Amylose Agarose (NEB, France), according to each manufacturer's instructions. The probes were biotin end-labeled according to the instructions of the Biotin 3' End DNA Labeling kit (Pierce, #89818, Thermo Fisher Scientific) and annealed to a double-stranded probe DNA. EMSA were performed according to the instructions of the Light Shift Chemiluminescent EMSA kit (Thermo Fisher Scientific, 20148). The DNA probes used in the EMSA are shown in *SI Appendix, Table S3*.

**Chromatin Immunoprecipitation (ChIP)-qPCR.** ChIP assay was carried out using the EpiQuik™ Plant ChIP Kit (Epigentek). Approximately 1.0 g of 4-d-old seedlings were harvested from *SIHY5*-HA-OE and *pSIPIF4*: *SIPIF4*-GFP plants. Chromatin was immunoprecipitated with anti-HA antibody (Abcam, ab18181, UK) and anti-GFP antibody. The goat anti-mouse IgG antibody (Abcam, ab205719, UK) was used as the negative control. ChIP-qPCR was performed with specific primers as shown in *SI Appendix, Table S4*.

**Dual-Luciferase Assay.** Dual-luciferase assays were performed as previously described (41). The full-length coding region of *SIHY5* or *SIPIF4* was amplified and fused to the pAC007 vector, while the promoters of *SICPK27* and *SIDWF* were cloned into the pGreen II 0800-LUC vector. The primers used are listed in *SI Appendix, Table S2*. *A. tumefaciens* strain GV3101 containing the vectors was resuspended in infiltration buffer (150  $\mu$ M acetosyringone, 10 mM MES, and 10 mM MgCl<sub>2</sub>, pH 5.6) and adjusted to a concentration of OD<sub>600</sub> = 0.7 to 0.8. Then, the mixture of the Agrobacterium containing pAC007 vector or pGreen II 0800-LUC suspensions (10:1, v:v) was infiltrated into *N. benthamiana* leaves. The activities of firefly luciferase (LUC) and Renilla luciferase (REN) were assayed 2 d after infiltration by using DualLuci<sup>®</sup> Firefly & Renilla Assay Kit (F6075, US EVERBRIGHT, Suzhou, China) and a modulus luminometer (Promega). The LUC/REN value in the absence of *SIHY5* or *SIPIF4* protein was set as one, and the analyses were performed with four replicates.

**Protein-Protein Interaction Assays.** The Y2H assay utilized the Matchmaker GAL4 Two-Hybrid System from Clontech. The process involved inserting the full-length coding sequences (CDS) of *SIPIF4* into the pGADT7 vector, while those of *SICPK27* were inserted into the pGBKT7 vector. These constructs, serving as bait and prey, were introduced into the yeast strain AH109 and cultured on synthetic dropout SD/-Trp/-Leu medium (provided by Coolaber Biotech Co., LTD, China). Colonies were then transferred to SD/-His/-Leu/-Trp solid medium to facilitate the selection of interactions.

In the BiFC assay, constructs containing 2YN-SIPIF4 or 2YN-SIPIF3 and 2YC-SICPK27 were transiently expressed in *N. benthamiana* leaves. This expression was accomplished by infiltrating Agrobacterium suspension (OD<sub>600</sub> = 1.0) into the leaves using a needleless syringe. Following inoculation for 48 h, fluorescence images were captured by a confocal laser scanning microscope (Zeiss LSM 780, Germany).

In the pull-down assay, the interaction between proteins was assessed by incubating 1.5  $\mu$ g of GST or GST-SIPIF4 prey proteins with 1.5  $\mu$ g of His-SICPK27 bait proteins in a binding buffer as we previously reported (44). This mixture was then added to GST resin (TransGen Biotech, DP201-01, China) and rotated for 2 h at 4 °C. Afterward, the beads were washed 4 times using the same binding buffer, and the pulled-down proteins were detected by immunoblotting using anti-His and anti-GST antibodies.

For co-IP assay, SIPIF4-GFP or empty vectors and SICPK27-Flag were transiently expressed in *N. benthamiana* by infiltrating Agrobacterium suspension (OD<sub>600</sub> = 1) into leaves using needle-less syringes. 2 d later, the leaves were pretreated with 200  $\mu$ M MG132 and then inoculated with 15 mM CaCl<sub>2</sub> or dH<sub>2</sub>O as a control for 2 h before sampling. The co-IP assay was performed as previously described (44). Briefly, the samples were ground into powder and mixed with 500  $\mu$ L of co-IP buffer. After centrifugation, 300  $\mu$ L of supernatant was collected and incubated with 10  $\mu$ L of GFP-beads (LABELAD Inc., China) at 4 °C for 3 h. After washing the beads 4 times, and the immunoprecipitated proteins were detected using anti-GFP and anti-Flag antibodies in western blotting assays.

**Phosphorylation Assays.** To identify the phosphosites of SIPIF4, the LC-MS/MS analysis was applied by APTBIO Co. Ltd. (Shanghai, China). Briefly, purified His-SICPK27 and MBP-SIPIF4 were first incubated in kinase buffer (25 mM Tris-HCl, 10 mM MgCl<sub>2</sub>, pH 7.5, 0.1 mM CaCl<sub>2</sub>, 0.2 mM ATP, and 1 mM DTT). This mixture was gently shaken for 3 h at 25 °C to allow phosphorylation to occur. The reaction was then halted by adding 4  $\times$  SDS loading buffer. Next, MBP-SIPIF4 was collected and separated by SDS-PAGE. The separated MBP-SIPIF4 bands were subjected to in-gel digestion by trypsin for 8 h. The resulting phosphopeptides were then analyzed using LTQ Orbitrap Elite (Thermo-Fisher) for further MS analysis, allowing for the identification of specific phosphosites on SIPIF4.

The Phos-tag mobility shift assay was performed according to a previous study with minor modifications (45). Briefly, after in vitro phosphorylation reaction, the proteins were separated in a 10% (w/v) SDS-PAGE gel, which contained 50 mM Phos-tag and 200 mM MnCl<sub>2</sub>. After electrophoresis, transfer buffer (50 mM Tris, 10 mM of EDTA, and 40 mM Gly) was used to wash the gel for 3 times (10 min for each wash), and the gel was washed for another 10 min using transfer buffer without EDTA. After transfer to polyvinylidene fluoride membrane, the phosphorylated SIPIF4 protein was detected by the MBP antibody.

For in vivo phosphorylation assay, the SIPIF4-Flag and SICPK27-GFP were co-expressed in *N. benthamiana* leaves for 2 d. To explore the effect of Ca<sup>2+</sup> on SICPK27-mediated phosphorylation of SIPIF4, the *N. benthamiana* leaves pretreated with 200  $\mu$ M MG132 were inoculated in 15 mM CaCl<sub>2</sub> or dH<sub>2</sub>O control for 2 h before the sampling. To examine how light influences SICPK27-mediated SIPIF4 phosphorylation, the leaves pretreated with 200  $\mu$ M MG132 and 200  $\mu$ M cyclohexamide (CHX, a protein synthesis inhibitor) were transferred to white light for 2 h before the sampling. The samples were ground into powder and mixed with co-IP buffer. After centrifugation, the supernatant was collected and incubated with GFP-Beads (LABELAD Inc., China) or Flag-Beads (SB-PR002, Share-bio, Shang Hai). After rotating at 4 °C for 3 h, the proteins were analyzed using anti-pSer/pThr antibody (ECM Biosciences, PM3801) or anti-pSer antibody (Santa Cruz Biotechnology, sc-81514) in the western blotting assays.

The SICPK27 kinase activity assay was performed according to Zhao et al. (46) with minor modifications. Briefly, *N. benthamiana* leaves overexpressing SICPK27-GFP were exposed to white light in the presence of 200  $\mu$ M CHX for different times or were subjected to pharmacological treatments (15 mM CaCl<sub>2</sub>, 20 mM EGTA, 10 mM LaCl<sub>3</sub>, or dH<sub>2</sub>O control), respectively. The leaves were ground into powder in liquid nitrogen and then mixed with co-IP buffer to extract total soluble proteins. The supernatant was collected and incubated with GFP-Beads (LABELAD Inc., China) for enrichment of the GFP-tagged SICPK27 protein. Kinase assays were performed by incubating the immunoprecipitated SICPK27-GFP and 15 ng MBP-SIPIF4 substrate protein in 50  $\mu$ L kinase buffer at 25 °C for 2 h. The reactions were stopped by adding 50  $\mu$ L  $\times$  SDS loading buffer. Phosphorylated proteins were detected by anti-pSer/pThr antibody in western blotting assays.

**Cell-Free Protein Degradation Assay.** Cell-free protein degradation assay was conducted as previously reported by Yu et al. (22) with minor modifications. Briefly, total proteins were extracted from the 4-d-old WT seedlings using the extraction buffer. The recombinant MBP-SIPIF4 protein and its variants were then incubated in the total protein extracts. The mixture was incubated at 25 °C for indicated periods, and the proteins were collected and separated by SDS-PAGE. The recombinant MBP-SIPIF4 protein and its variants were detected by immunoblot with anti-MBP antibody.

**Cell Fractionation.** The *proSICPK27*: *SICPK27*-GFP were transiently expressed in *N. benthamiana* leaves for 2 d in the dark. The leaves of *N. benthamiana* were harvested before and after transfer to light conditions (100  $\mu$ mol m<sup>-2</sup> s<sup>-1</sup>) for 3 and 6 h. The fractionation assay was performed as previously described with modifications (47). Briefly, samples were ground in liquid nitrogen and homogenized in lysis buffer [300 mM sucrose, 20 mM Tris-HCl (pH 8.0), 5 mM MgCl<sub>2</sub>, 5 mM KCl, 0.3% Triton X-100, 5 mM NP-40, 5 mM-mercaptoethanol, and 35% glycerol, 5 mM DTT, protease inhibitor cocktail]. The homogenates were filtered through two layers of Miracloth (Calbiochem) and then centrifuged at 5,000 g for 10 min at 4 °C, after which the supernatant was collected as cytosol fraction. The pellet was washed repeatedly with nuclear protein extraction buffer [50 mM Tris-HCl (pH 8.0), 10 mM EDTA, 1% SDS, 5 mM DTT, and protease inhibitor cocktail] until the green pellet became white, which corresponds to the nuclear fraction. Then cytosol and nuclear fractions were boiled in 5  $\times$  SDS loading buffer at 95 °C for 10 min before immunoblot analysis. The proteins were detected with antibodies against GFP, cytoplasmic marker phosphoenolpyruvate carboxylase (PEPC) (Agrisera, AS09 458, Sweden), and nuclear marker histone H3 (Millipore, 05-499).

**Statistical Analysis.** For measuring hypocotyl length, unless otherwise mentioned at least 15 seedlings (n, individual dots) were used. Other bar diagrams show the mean of three or four independent biological replicates (n, individual dots). Data were statistically analyzed by ANOVA using GraphPad InStat software 8.3.0 for Windows (GraphPad Software Inc., La Jolla, CA) and R software. The

significance of treatment differences was analyzed using ANOVA followed by Tukey's test or Student's test.

**Data, Materials, and Software Availability.** All study data are included in the article and/or [supporting information](#).

**ACKNOWLEDGMENTS.** We are thankful to Dr. X.D. Wu for the help in phytohormones analysis and Dr. Z.Y. Qi for the maintenance of the growth chambers. We also thank Dr. C.X. Liu for his inspiration for our project. This work was supported by National Natural Science Foundation of China (32330094,

32372790, 323B2057), the Modern Agro-industry Technology Research System of China (CARS-25-02A), the Starry Night Science Fund of Zhejiang University Shanghai Institute for Advanced Study (SN-ZJU-SIAS-0011).

Author affiliations: <sup>a</sup>Department of Horticulture, Zhejiang University, Hangzhou 310058, China; <sup>b</sup>Hainan Institute, Zhejiang University, Yazhou Bay Science and Technology City, Sanya 572025, China; <sup>c</sup>Key Laboratory of Horticultural Plant Growth and Development, Agricultural and Rural Ministry of China, Zhejiang University, Hangzhou 310058, China; and <sup>d</sup>School of Biosciences, College of Life and Environmental Sciences, University of Birmingham, Edgbaston B15 2TT, United Kingdom

1. C. Kami, S. Lorrain, P. Hornitschek, C. Fankhauser, Light-regulated plant growth and development. *Curr. Top. Dev. Biol.* **91**, 29–66 (2010).
2. J. Dong, W. Terzaghi, X. W. Deng, H. D. Chen, Multiple photomorphogenic repressors work in concert to regulate Arabidopsis seedling development. *Plant Signal. Behav.* **10**, e1011934 (2015).
3. R. Podolec, R. Ulm, Photoreceptor-mediated regulation of the COP1/SPA E3 ubiquitin ligase. *Curr. Opin. Plant Biol.* **45**, 18–25 (2018).
4. X. Han, X. Huang, X. W. Deng, The photomorphogenic central repressor COP1: Conservation and functional diversification during evolution. *Plant Commun.* **1**, 100044 (2020).
5. H. Zhao, Y. Bao, PIF4: Integrator of light and temperature cues in plant growth. *Plant Sci.* **313**, 111086 (2021).
6. X. S. Xu, I. Paik, L. Zhu, E. Huq, Illuminating progress in phytochrome-mediated signaling pathways. *Trends Plant Sci.* **20**, 641–650 (2015).
7. T. Y. Delormel, M. Boudsocq, Properties and functions of calcium-dependent protein kinases and their relatives in Arabidopsis thaliana. *New Phytol.* **224**, 585–604 (2019).
8. G. Baum, J. C. Long, G. I. Jenkins, A. J. Trethewas, Stimulation of the blue light phototropic receptor NPH1 causes a transient increase in cytosolic Ca<sup>2+</sup>. *Proc. Natl. Acad. Sci. U.S.A.* **96**, 13554–13559 (1999).
9. Neuhaus, Calcium/calmodulin-dependent and calcium/calmodulin-independent phytochrome signal-transduction pathways (Vol 73, pg 937, 1993). *Cell* **79**, 743–743 (1994).
10. Y. Zhao *et al.*, Sensory circuitry controls cytosolic calcium-mediated phytochrome B phototransduction. *Cell* **186**, 1230–1243.e14 (2023).
11. S. N. Gangappa, J. F. Botto, The Multifaceted roles of HY5 in plant growth and development. *Mol. Plant* **9**, 1353–1365 (2016).
12. C. Zhu *et al.*, Phosphorylation of sugar transporter TST2 by protein kinase CPK27 enhances drought tolerance in tomato. *Plant Physiol.* **195**, 1005–1024 (2024).
13. S. Bernardo-Garcia *et al.*, BR-dependent phosphorylation modulates PIF4 transcriptional activity and shapes diurnal hypocotyl growth. *Genes Dev.* **28**, 1681–1694 (2014).
14. S. N. Gangappa, S. V. Kumar, DET1 and HY5 control PIF4-mediated thermosensory elongation growth through distinct mechanisms. *Cell Rep.* **18**, 344–351 (2017).
15. Z. Y. Wei *et al.*, Brassinosteroid biosynthesis is modulated via a transcription factor cascade of COG1, PIF4, and PIF5. *Plant Physiol.* **174**, 1260–1273 (2017).
16. E. Park, Y. Kim, G. Choi, Phytochrome B requires pif degradation and sequestration to induce light responses across a wide range of light conditions. *Plant Cell* **30**, 1277–1292 (2018).
17. P. Leivar, P. H. Quail, PIFs: Pivotal components in a cellular signaling hub. *Trends Plant Sci.* **16**, 19–28 (2011).
18. K. A. Franklin *et al.*, Phytochrome-interacting factor 4 (PIF4) regulates auxin biosynthesis at high temperature. *Proc. Natl. Acad. Sci. U.S.A.* **108**, 20231–20235 (2011).
19. D. Rosado *et al.*, Downregulation of phytochrome-interacting factor 4 influences plant development and fruit production. *Plant Physiol.* **181**, 1360–1370 (2019).
20. W. Sun *et al.*, Mediator subunit MED25 physically interacts with phytochrome interacting factor 4 to regulate shade-induced hypocotyl elongation in tomato. *Plant Physiol.* **184**, 1549–1562 (2020).
21. C. Ibanez *et al.*, Brassinosteroids dominate hormonal regulation of plant thermomorphogenesis via BZR1. *Curr. Biol.* **28**, 303 (2018).
22. Z. Yu *et al.*, Auxin promotes hypocotyl elongation by enhancing BZR1 nuclear accumulation in Arabidopsis. *Sci. Adv.* **9**, eade2493 (2023).
23. X. J. Li *et al.*, DWARF overexpression induces alteration in phytohormone homeostasis, development, architecture and carotenoid accumulation in tomato. *Plant Biotechnol. J.* **14**, 1021–1033 (2016).
24. J. H. Jung *et al.*, Phytochromes function as thermosensors in Arabidopsis. *Science* **354**, 886–889 (2016).
25. J. J. Casal, S. Balasubramanian, Thermomorphogenesis. *Annu. Rev. Plant Biol.* **70**, 321–346 (2019).
26. X. Xu *et al.*, Distinct light and clock modulation of cytosolic free Ca<sup>2+</sup> oscillations and rhythmic chlorophyll a/b binding protein 2 promoter activity in Arabidopsis. *Plant Cell* **19**, 3474–3490 (2007).
27. X. Zhao *et al.*, Phototropins function in high-intensity blue light-induced hypocotyl phototropism in Arabidopsis by altering cytosolic calcium. *Plant Physiol.* **162**, 1539–1551 (2013).
28. Q. Y. Bu *et al.*, Phosphorylation by CK2 enhances the rapid light-induced degradation of phytochrome interacting factor 1 in Arabidopsis. *J. Biol. Chem.* **286**, 12066–12074 (2011).
29. W. M. Ni *et al.*, PPKs mediate direct signal transfer from phytochrome photoreceptors to transcription factor PIF3. *Nat. Commun.* **8**, 15236 (2017).
30. X. Y. Xin *et al.*, Arabidopsis MKK10-MPK6 mediates red-light-regulated opening of seedling cotyledons through phosphorylation of PIF3. *J. Exp. Bot.* **69**, 423–439 (2018).
31. H. Li, E. S. Burgie, Z. T. K. Gannam, H. Li, R. D. Vierstra, Plant phytochrome B is an asymmetric dimer with unique signalling potential. *Nature* **604**, 127–133 (2022).
32. C. Martínez *et al.*, PIF4-induced BR synthesis is critical to diurnal and thermomorphogenic growth. *EMBO J.* **37**, e99552 (2018).
33. Y. H. Hao *et al.*, Green means go: Green light promotes hypocotyl elongation via brassinosteroid signaling. *Plant Cell* **35**, 1304–1317 (2023).
34. L. J. Qi, Y. T. Shi, W. Terzaghi, S. H. Yang, J. G. Li, Integration of light and temperature signaling pathways in plants. *J. Integr. Plant Biol.* **64**, 393–411 (2022).
35. C. Delker *et al.*, The DET1-COP1-HY5 pathway constitutes a multipurpose signaling module regulating plant photomorphogenesis and thermomorphogenesis. *Cell Reports* **9**, 1983–1989 (2014).
36. Y. J. Park, H. J. Lee, J. H. Ha, J. Y. Kim, C. M. Park, COP1 conveys warm temperature information to hypocotyl thermomorphogenesis. *New Phytol.* **215**, 269–280 (2017).
37. Z. W. Zhao *et al.*, CRY2 interacts with CIS1 to regulate thermosensory flowering via FLM alternative splicing. *Nat Commun.* **13**, 1045 (2022).
38. S. Kim *et al.*, The epidermis coordinates thermoresponsive growth through the phyB-PIF4-auxin pathway. *Nat Commun.* **11**, 1053 (2020).
39. L. D. Vu *et al.*, The membrane-localized protein kinase MAP4K4/TOT3 regulates thermomorphogenesis. *Nat. Commun.* **12**, 2842 (2021).
40. S. B. Ge *et al.*, Light-dependent activation of HY5 promotes mycorrhizal symbiosis in tomato by systemically regulating strigolactone biosynthesis. *New Phytol.* **233**, 1900–1914 (2022).
41. H. Dong *et al.*, HY5 functions as a systemic signal by integrating BRC1-dependent hormone signaling in tomato bud outgrowth. *Proc. Natl. Acad. Sci. U.S.A.* **120**, e2301879120 (2023).
42. S. X. Ge, D. Jung, R. Yao, ShinyGO: A graphical gene-set enrichment tool for animals and plants. *Bioinformatics* **36**, 2628–2629 (2019).
43. R. A. M. Villanueva, Z. J. Chen, ggplot2: Elegant Graphics for Data Analysis. *Meas.-Interdiscip. Res. Perspectives* **17**, 160–167 (2019).
44. Z. Hu *et al.*, The protein kinase CPK28 phosphorylates ascorbate peroxidase and enhances thermotolerance in tomato. *Plant Physiol.* **186**, 1302–1317 (2021).
45. K. Ye *et al.*, BRASSINOSTEROID-INSENSITIVE2 negatively regulates the stability of transcription factor ICE1 in response to cold stress in Arabidopsis. *Plant Cell* **31**, 2682–2696 (2019).
46. M. Zhao *et al.*, The osmotic stress-activated receptor-like kinase DYP1 mediates SnRK2 kinase activation and drought tolerance in Setaria. *Plant Cell* **35**, 3782–3808 (2023).
47. Y. Ding *et al.*, CPK28-NLP7 module integrates cold-induced Ca<sup>2+</sup> signal and transcriptional reprogramming in Arabidopsis. *Sci. Adv.* **8**, eabn7901 (2022).